POLITECNICO DI TORINO
Repository ISTITUZIONALE

Theoretical evaluation of the evaporation rate of 2D solar-driven interfacial evaporation and of its large-scale application potential

Original
Theoretical evaluation of the evaporation rate of 2D solar-driven interfacial evaporation and of its large-scale application potential / Song, Z.; Tiraferri, A.; Yuan, R.; Cao, J.; Tang, P.; Xie, W.; Crittenden, J. C.; Liu, B.. - In: DESALINATION. - ISSN 0011-9164. - 537:(2022), p. 115891. [10.1016/j.desal.2022.115891]

Availability:
This version is available at: 11583/2969573 since: 2022-07-06T09:21:48Z

Publisher:
Elsevier B.V.

Published
DOI:10.1016/j.desal.2022.115891

Terms of use:

This article is made available under terms and conditions as specified in the corresponding bibliographic description in the repository

Publisher copyright

(Article begins on next page)

21 January 2025

In preparation for ***Desalination***

Date: *May 23, 2022*

Theoretical evaluation of the evaporation rate of 2D solar-driven interfacial evaporation and of its large-scale application potential

Zhaoyang Song [a,b,c], *Alberto Tiraferri* [d], *Ruihong Yuan* [c], *Jinzhi Cao* [e], *Peng Tang* [a,b], *Wancen Xie* [a,b], *John C. Crittenden* [f], *Baicang Liu* [a,b,*]

[a] Key Laboratory of Deep Earth Science and Engineering (Ministry of Education), Institute of New Energy and Low-Carbon Technology, College of Architecture and Environment, College of Physics, Sichuan University, Chengdu, Sichuan 610207, PR China

[b] Yibin Institute of Industrial Technology, Sichuan University Yibin Park, Section 2, Lingang Ave., Cuiping District, Yibin, Sichuan 644000, PR China

[c] College of Physics, Sichuan University, Chengdu, Sichuan 610065, China

[d] Department of Environment, Land and Infrastructure Engineering, Politecnico di Torino, Corso Duca degli Abruzzi 24, 10129 Turin, Italy

[e] College of Computer Science, Sichuan University, Chengdu, Sichuan 610065, China

---

[*]Corresponding author. Tel.: +86-28-85995998; fax: +86-28-62138325; E-mail: bcliu@scu.edu.cn; baicangliu@gmail.com (B. Liu).

[f] Brook Byers Institute for Sustainable Systems, School of Civil and Environmental Engineering, Georgia Institute of Technology, Atlanta, GA 30332, USA

ABSTRACT

2D solar-driven interfacial evaporation (2D SIE) is a low-cost, environmentally friendly water treatment solution. Studies have improved the performance of single-stage evaporation close to its upper bound in controlled environments. However, the most critical parameter – the rate of evaporation – was only assessed by laboratory-scale measurements and data are typically obtained under a specific set of conditions. Previous studies did not evaluate or modeled evaporation rates in the case of changing environmental variables, for example, temperature, humidity, or wind speed. To effectively utilize the 2D SIE technology at real scale and understand its potential in different scenarios, the spatial and temporal variability of environmental parameters must be considered. To preliminarily address this issue, we propose the first model for assessing the evaporation rate of 2D SIE systems in real environments. Based on this theoretical model, we thus explore the potential deployment of the 2D SIE technology globally. This study provided a basis for further model development and it discusses key information to guide further improvements of 2D SIE systems design and its large-scale implementation.

Keywords: Interfacial evaporation; Solar desalination; 2D evaporator; Theoretical model; Global assessment

1. Introduction

Evaporation is a natural process, ubiquitous in nature, which separates water of high purity from contaminants and other substances (e.g., salts). However, heat utilization is inefficient during so-called bulk evaporation, with only about 20% of the energy directed to the phase change phenomenon, due to heat dissipation mechanisms [1]. Engineered evaporation relying on environmentally friendly, low-cost energy sources, such as solar energy, has gained momentum in the last decade within the overarching effort to provide affordable water treatment systems powered by renewable energy [2-4].

To solve the problem of inefficient energy utilization, thermal localization strategies have been proposed that effectively reduce heat loss and increase energy conversion by selectively confining the heating to the surface where phase change happens, instead of the entire water body [5]. Solar-driven interfacial evaporation (SIE) technology is the product of this broad concept [2]. According to the structure of the evaporator, the SIE systems are classified as 2D SIE and 3D SIE. Due to the advantages of simple structure, low cost, and simple maintenance, the 2D SIE system is considered to have great potential in practical application [6]. 2D SIE systems have shown outstanding success in the utilization of solar heat and achieved highly efficient energy conversion, so much so that they have even begun exceeding the apparent theoretical limit through mechanisms of absorption of the environmental heat and reuse of the latent heat [7-10]. Evaporation efficiencies around 90% have been shown with several materials, and higher water production rates than those predicted from calculations based on the pure phase change $(\sim 1.5\ kg\ m^{-2} h^{-1})$ have been reported [11-14]. Also, the quality of the condensed product that has been produced starting from waste liquid is typically high [14-16].

The availability of thermal positioning techniques and the efficiency leap driven by the innovation in materials have greatly enhanced the possibility of implementing the SIE technology at real scale. Nevertheless, the vast majority of research has so far stopped at the laboratory stage, and most of the experiments simulating real environments have generally been conducted at small-scale and for short durations, for demonstrative purposes only [11, 17]. Except for a few works, such as a recent one in which researchers have combined SIE with solar panels to apply this technology in large-scale industries [9], relevant industrial applications have not been reported. The current mainstream research trend in 2D SIE technology largely consists of developing new materials to improve the evaporation efficiency. This research commonly comprises small-scale characterization of new materials, which is insufficient to understand the large-scale applicability of the technology [18], a topic that has been not adequately explored so far. Also, differences in laboratory-scale experimental methodologies complicate comparison of the data obtained by different research efforts. Some researchers have provided experimental guidance to improve the availability and usability of laboratory data [19]. In Table S1 of the Supporting Information, we summarize the relevant data from some 2D SIE evaporators collected in the last four years (2019-2022). It is clear that many studies lack reports of some necessary parameters to understand the experimental conditions, highlighting the lack of standardization in the SIE research field [15, 20-28], which in turn impairs the practical implementation of this process.

The prospect of placing SIE technology to practical industrial use has been discussed in our previous article [29], where we reviewed the prospect of SIE technology in the field of industrial wastewater treatment, mainly focusing on cost, pointing out that the SIE technology is a competitive industrial water treatment solution under certain conditions. Many reports have also preliminarily discussed the potential promising application of SIE in other fields, such as high-quality water production and civil wastewater treatment [9, 13, 16, 29-31].

This study contributes to efforts aimed at increasing the feasibility of large-scale 2d SIE. We hypothesize that the application of 2D SIE technology for water treatment solutions can be adequately predicted taking into account variable environmental factors, thus improving predictions of the evaporation rate by considering the installation environment. A diagnostic model is designed and proposed, based on which the installation potential of 2D SIE on a global scale is estimated. Based on this model, we point out the current potential and needs of 2D SIE technology and research, including the need for accessible, interoperable, and reusable data, as well as the necessity of large-scale, long-term 2D SIE pilot tests.

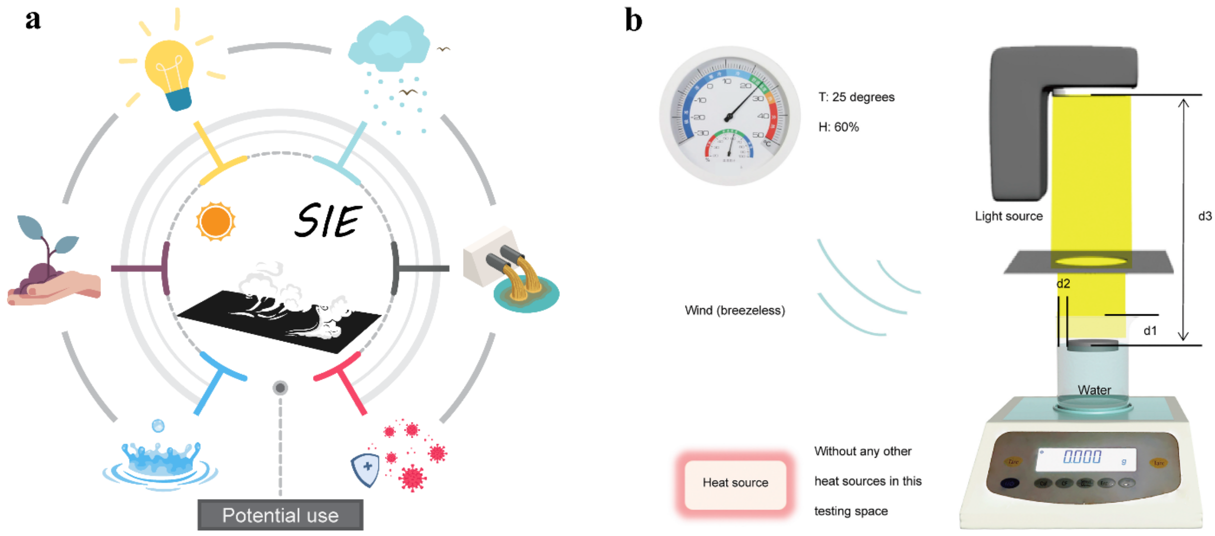

Figure 1. Potential applications of SIE technology and technical conventions employed in SIE research at this stage. (a) SIE technology has significant potential in areas including, from bottom left in the figure, desalination [15, 32], agricultural water improvement [29], solar steam power generation [9, 31], possible means on climate improvement [33], industrial wastewater treatment [29], and solar steam disinfection [1, 30]. (b) Some technical conventions for SIE experimental materials and systems under laboratory conditions, including specification of temperature, relative humidity, wind speed, and other conditions [Fig1.(b) revised with permission from ref [19]].

2. Assessing the industrial application of 2D SIE technology: prediction on evaporation rate

Evaluations of cost and efficiency are required before the 2D SIE technology is rolled out on a large scale and to determine if stakeholders would consider this solution as an option for future applications. Detailed calculations of the cost of 2D SIE technology is complex and case-specific, as it requires considering all service costs, such as infrastructure inputs, materials transportation, labor, and many others. However, a preliminary conservative estimate in our previous work indicated that the cost of SIE technology might be significantly lower than that of conventional membrane/thermal-based technologies used in the same desalination applications, specifically, below or around $1 per cubic meter of product water [29]. Here, we focus our attention on the issue of efficiency, namely, evaporation rate, the other decisive factor in determining whether the technology may become a feasible one in the portfolio of water treatment options.

2.1 Calculation of evaporation volume and evaporation efficiency under laboratory conditions

The SIE efficiency under standard conditions (1 sun irradiation) is calculated with the following equation [5, 15, 34-36]:

$$\eta = \frac{\dot{m} h_V}{C_{opt} P_0} \#(1)$$

where η denotes the evaporation efficiency, $\dot{m}$ denotes the water vapor mass flux (unit chosen as $kg \cdot m^{-2} \cdot h^{-1}$), h_V denotes the enthalpy of evaporation of water ($J \cdot kg^{-1}$), P_0 denotes solar radiation power of 1 sun ($1\, kW \cdot m^{-2}$), and C_{opt} denotes the optical concentration of the absorber surface.

As depicted in Fig. 1(b), laboratory experimenters follow certain general conventions to artificially eliminate the effects of temperature, air humidity, wind [19]. While evaporation efficiency is the best parameter to allow comparison of the performance of different systems and materials investigated under laboratory conditions, evaporation rate is a better indicator to evaluate the evaporation process in field scenarios and to obtain a more quantitative prediction of the performance of SIE technology at large-scale, where wind and air humidity significantly influence the net energy input.

2.2 Evaporation prediction model for 2D SIE technology based on evapotranspiration related theory and Penman formula extension

The water evaporation process at the earth's surface, the transpiration of plant leaves, and the sublimation of snow and ice are known collectively as evapotranspiration in the field of meteorology [37-41]. The description of the evapotranspiration process may be used as a blueprint for the description of the 2D SIE performance, since evaporation in a real environment requires consideration of four main meteorological variables, namely, the wind speed, atmospheric humidity, radiation, and air temperature, similar to natural evaporation processes studied in meteorology and agriculture [40, 41].

To obtain an accurate description of the evaporation in the SIE technique, we make certain extensions to the Penman formula for estimating evaporation from open water surfaces and the Penman-Monteith formula for estimating evapotranspiration, both of which are semi-empirical relationships for meteorological factors that have been verified by a large amount of data and regarded as highly reliable [42, 43]. Our modified formula follows Penman's consideration of energy conservation and heat and mass transfer relationships [42], and proposes a correction for the specific behavior of 2D SIE with respect to natural evaporation or plant transpiration. We express the theoretical evaporation rate with the following equation:

$$ET = \frac{(\Delta \cdot R_n \cdot 0.9) + \frac{\rho c_p (e_s(T) - e)}{r_H}}{\lambda \cdot (\Delta + \gamma)} \times U_t \quad \#(2)$$

where ET denotes the theoretical evaporation rate, Δ denotes the slope of the saturation vapor pressure-temperature relationship, R_n denotes the net radiation, ρ represents the average air density at the ambient pressure corresponding to the evaporation process, c_p

denotes the specific heat capacity of air at constant pressure, $e_s(T)$ represents the saturated vapor pressure at temperature T, e represents the actual vapor pressure in the air, r_H denotes the aerodynamic resistance that is determined by the evaporation surface, λ denotes the enthalpy of evaporation of water, γ denotes the humidity constant, and U_t is unit conversion constant which depends on the units of each physical quantity chosen by the user when using this formula. The derivation of Equation (2) can be found in the Supporting Information (SI). The physical basis of the formula is the energy conservation equation of the evaporating surface with the overall mass transfer characteristics of the turbulent boundary layer.

All the parameters in Equation (2) can be each ultimately expressed as a functional relationship of the same five input environmental variables,

$$ET = f(R_n, u_z, e, T, P) \quad \#(3)$$

where ET denotes the theoretical evaporation rate, R_n denotes the net radiation, u_z denotes the wind speed measured at height z meters (a common meteorological parameter), e denotes the actual vapor pressure in the air, T denotes the temperature of the air, P denotes the atmospheric pressure. See SI for expressions of the specific dependency of each parameter on the environmental variables, many of which are empirical in nature.

As outlined in the SI, we introduce the concept of "reference evaporation surface" during derivation. This step is useful to simplify the choice among a wide variety of evaporation surfaces characterized by specific heat transfer characteristics, heat loss caused by long-wave radiation, shape and roughness, and other potentially diverse properties. The "reference evaporation surface" is set by assigning values to a specific set of parameters related to the device configuration and characteristics, mainly concerning the height of the evaporation surface and the surface physical properties. In particular, the "reference evaporation surface" represents here a material and configuration based on recent reports of state-of-the-art porous media applied in 2D SIE. This surface is a relevant example for this field, but may also be regarded as a reference basis for comparison o other materials and systems that are being developed. If relevant, users can apply the model presented here to different surfaces by adjusting the parameters related to the surface characteristics. See SI for specific assumptions.

Different reference evaporation surfaces may be used in different calculation sets, as long as the characteristics of the material and surface are known. Also note that changes in water salinity will also slightly affect the evaporation rate, but this study did not introduce this variable into the model. At the same time, we did not consider the reduction of latent heat due to the coupling of the material to water. The properties of enthalpy changes in 2D materials obey the descriptions of semi-empirical physical formulas. The salinity of the target water body involved in the 2D SIE technology is typically large. However, for water bodies with ultra-high salinity, a correction factor should be used, which depends on the actual salt content [44].

2.3 Sensitivity analysis and brief discussion of the model

Modeling of the evaporation rate incorporates the consideration of energy conservation and mass transfer processes in real situations, introducing several variables as uncertainty factors (the changes of which affect the evaporation rate). To understand the effect of variables and the robustness of the model, we first performed a sensitivity analysis of the equations presented in Section 2.2. We used the Sobol method to perform a global sensitivity analysis on our model, and the specific implementation of the analysis was conducted with Python's SALib library [45]. We selected the parameters of atmospheric pressure in the range of 80-103 kPa, temperature in the range of 0-40 °C, radiation in the range of 0-1.5 sun, wind speed in the range of 0-3 m s^{-1}, and relative humidity in the range of 60%-100%.

Therefore, we obtained the first-order sensitivity index and total-order index, where we found that about 50.9% of the output variance in the set analysis range is caused by the radiation intensity, about 19.4% of the output variance is caused by the wind speed, about 19.4% of the output variance is caused by the change of air humidity, about 19.2% of the output variance is caused by temperature, and only about 0.17% of the output variance is caused by pressure.

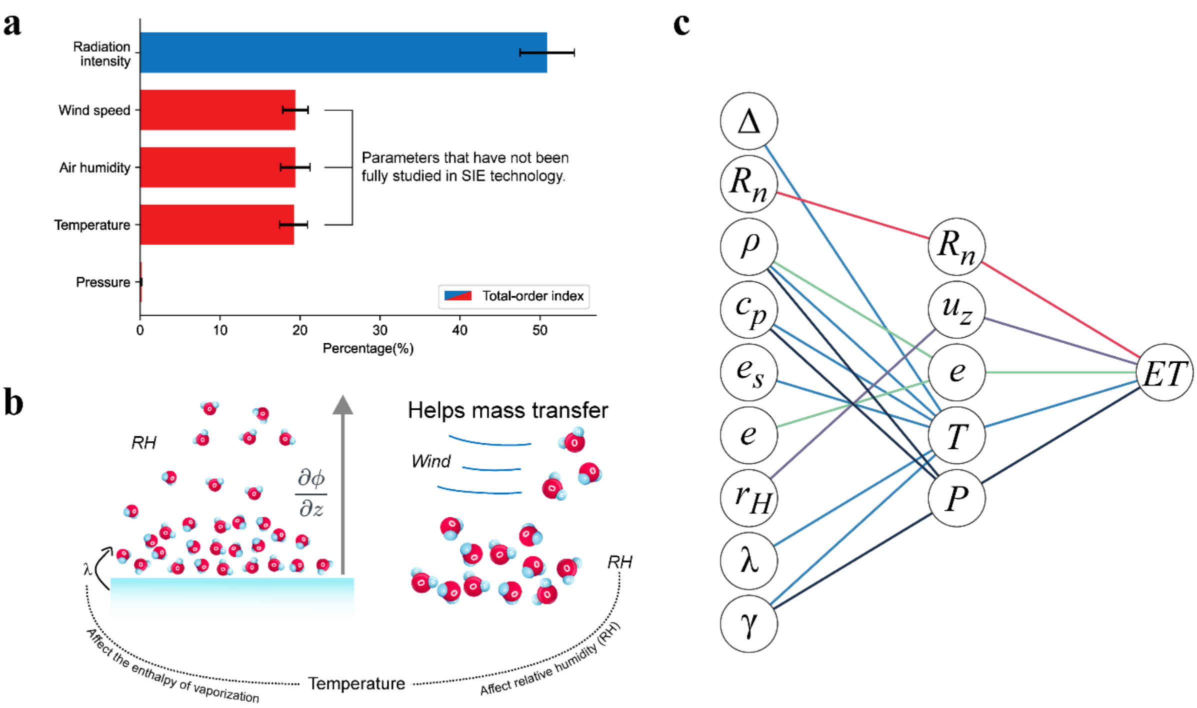

Figure 2. The influence of multiple variables on evaporation. (a) Total-order index calculated within the range of parameters. (b) How environmental parameters qualitatively affect the evaporation process: The principle of evaporation is that water molecules have sufficient kinetic energy to escape the water surface. In SIE technology, the surface material directly provides kinetic energy for water molecules based on the heat energy obtained from the photothermal conversion process. At the same time, the air's capacity for water molecules is limited. If humidity reaches saturation, the evaporation process will stop. The air humidity is proportional to the concentration of water molecules, that is, the higher the concentration of water molecules, the higher the humidity. In the figure, ϕ represents the concentration of water molecules, and $\partial\phi / \partial z$ represents the concentration gradient of water molecules in the vertical direction. Wind can help water vapor transport away from the water surface, reduces the concentration of water molecules near the surface of the liquid, increases the concentration gradient, and enhances the mass transfer process. Temperature will affect the enthalpy of vaporization and the saturated vapor pressure of air (i.e., relative humidity). (c) There is a certain empirical relationship between the physical quantities in Equation (2) and Equation (3). Both forms can provide the predicted value of ET. The network diagram shows the functional relationship between related physical quantities. The specific functional relationship can be found in SI.

Fig. 2(c) schematically presents the functional relationship between the parameters appearing in the model and the relationship between environmental parameters and ET. If water vapor is not transferred away from the evaporation surface, the accumulation of water vapor will negatively affect the evaporation process: air humidity and wind speed significantly affect the water gradient at the surface-air interface, thus the overall evaporation rate. Furthermore, local temperature affects the value of saturated vapor pressure and latent heat of vaporization. The specific functional relationship is presented in the SI, but in general, increasing temperature will increase the saturated vapor pressure and reduce the enthalpy of vaporization. The lower the value of the enthalpy of evaporation, the easier it is for the water to undergo phase change. The saturated vapor pressure represents the capacity of the air to hold water vapor. If the saturated vapor pressure is higher, the evaporation process will be more likely to occur. In this way, the temperature exerts an influence on the evaporation process.

Note that wind speed, temperature, and air humidity together are more important than radiation intensity in influencing evaporation rate and should not be overlooked. If researchers can exploit environmental wind to enhance the mass transfer process at the surface with a suitable design, or combine it with water-absorbing materials to change the concentration of water molecules near the surface, the evaporation rate would increase without additional energy input. We would like to underline that the complexity of the evaporation process leads to the fact that its exact mechanism is not yet fully understood. In addition to the inherent drawbacks in the derivation of the equations due to assumptions and approximations, the model proposed in this study is phenomenological, thus its output depends strongly on the accuracy of the estimation of the model parameters and other data measurements. It should thus be regarded as a user-friendly first approximation of the evaporation rate under different environmental conditions.

3. Estimating the potential of 2D SIE technology on a global scale based on theoretical formulas

3.1 Global Assessment

Applying the model formulation as described above in Section 2.2, we used reanalysis data provided by NASA [46], which has a spatial resolution of 0.1° × 0.1° (equivalent to 5 million data points), a temporal resolution of one month, and involves a latitude range of 60° S to 90° N. We used one year of data from the dataset for 2020, and obtained the model outputs based on the 2020 weather conditions for the global-scale 2D SIE technical evaporation potential. The results are presented in terms of total annual evaporation per unit area in Fig. 3(a).

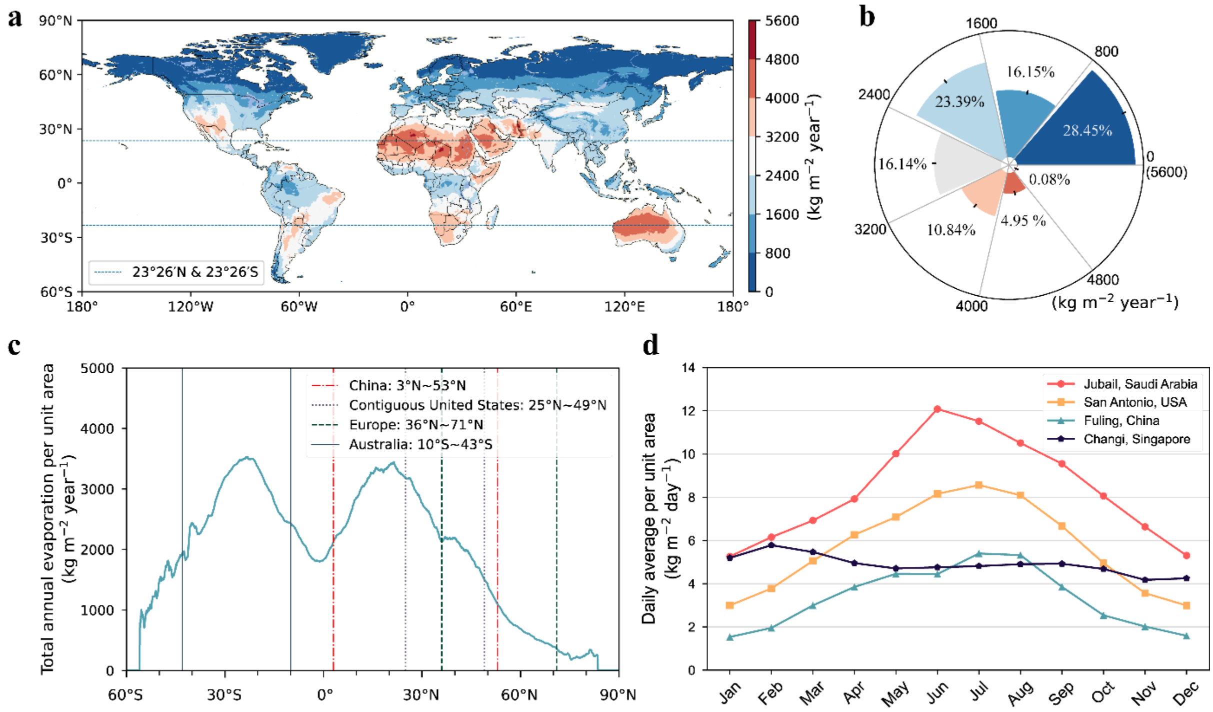

Figure 3. The global-scale 2D SIE technical evaporation potential prediction is calculated based on the theoretical model combined with global meteorological data for 2020 [46]. (a) The figure shows the global distribution of the predicted evaporation potential, calculated as the value of evaporation per unit area predicted to be generated in one year, with the evaporation unit as kg m^{-2} year^{-1}. (b) Percentage of data volume of each evaporation data segment: 100% represents the total considered land area, covering almost all regions of the globe except for the continent of Antarctica and some islands south of 60°S latitude. (c) The total annual evaporation per unit area varies with latitude: the mean value is calculated as the average value of the estimated evaporation of all land at a certain latitude. There are two peaks in the curve, mainly indicating the latitudes corresponding to the tropics and encompassing Australia and North Africa. The graph also indicates the latitudinal span of China, the Contiguous United States, Australia, and Europe. (d) Trend of the recalculated daily average per unit area (kg m^{-2} year^{-1}) in different months for four selected locations.

Evaporation shows greater potential in regions at or around the Tropic of Capricorn and the Tropic of Cancer, where the estimated evaporation rate per unit area is mostly concentrated in the interval of 3200-5600 kg m^{-2} year^{-1}. According to our summary statistics, the map of the predicted evaporation shows the distribution reported in Fig. 3(b). This result indicates that the evaporation achievable applying the 2D SIE technology is considerable in a significant portion of the globe but it requires wise site selection. Further, in Fig. 3(c) we provide the relationship of the annual evaporation per unit area with latitude, and the curve shows a very specific bimodal shape. We also indicate the approximate latitudinal ranges of some countries or regions, namely, China, the Contiguous United States, and Australia, all three having large evaporation potential, as well as Europe, which is associated with inferior results due to its northerly location.

3.2 Evaporation in four relevant locations

Four locations were selected as examples and our model was used to computationally estimate the evaporation rate of water using 2D SIE technology. Al Jubail, San Antonio, and Fuling all have the need for brine desalination or wastewater treatment. Al Jubail in Saudi Arabia has a need for desalination to produce drinking water; Fuling in Chongqing, China, has a large amount of high-salinity squash wastewater that needs to be treated due to its booming food industry; and San Antonio in Texas, USA is located in the Eagle Ford, a famous shale gas producing area [47], where high salinity backwash from the shale gas industry is also one of the target wastewaters treatable by this 2D SIE technology. The climate of these three regions is somewhat different, another reason why they were chosen as case studies for analysis. The fourth region, Singapore, was chosen to show how the "depression" in the evaporation curve displayed in Fig. 3(c) is formed near the equator.

The estimated evaporation per unit area for the four regions as a function of month is shown in Fig. 3(d), and the total annual evaporation rates per unit area are reported in Table 1. The rates for three tropical locations, Al Jubail, San Antonio, and Fuling, are substantial.

Even in Fuling, where environmental conditions are less favorable, the unit area is still capable of handling about one ton of water per year. It should be emphasized that as specific technologies advance, actual yields will further increase from this conservative value, possibly making the 2D SIE technology even more competitive.

Table 1. General weather data for Jubail (Saudi Arabia), San Antonio (USA), Fuling (China), and Changi (Singapore) (the specific data are provided in the SI, Table S3). The final row of the table is the estimated annual water production per unit area (kg m^{-2} $year^{-1}$).

Parameter	Jubail, Saudi Arabia	San Antonio, USA	Fuling, China	Changi, Singapore
Köppen climate classification [48]	BWh *	Cfa **	Cfa **	Af ***
Annual average wind speed (m s^{-1})	4.5	3.4	2.3	1.7
Annual average relative humidity (%)	59.00%	68.70%	75.10%	83.30%
Annual average temperature (°C)	26.1	20.0	16.5	26.7
Annual solar radiation – horizontal (MJ m^{-2} $year^{-1}$)	7332.85	6077.00	3949.30	5843.65
Annual water production per unit area (kg m^{-2} $year^{-1}$)	3043	2077	1219	1780

Note:

* BWh: hot desert climates;

** Cfa: humid subtropical climate;

*** Af: tropical rainforest climate.

Turning to the case of Singapore, the weather condition can be roughly understood from Table 1, where we find that although Singapore has a notable annual average temperature and radiation, its climate also corresponds to a high average humidity, which directly limits the evaporation process. The area around 10 to 15 degrees near the equator is mostly a tropical rainforest climate, a climate characterized by high temperatures, rain and humidity throughout the year, according to the Köppen climate classification [48]. The high humidity causes the depression of the predicted evaporation near the equator in the curve displayed in Fig. 3(c).

3.3 Interpretation of the numerical results

Based on the results of the model, we were able to obtain an approximate but intuitive understanding of the implementation potential of the 2D SIE technique, which shows an axisymmetric bimodal structure with the change of latitude in space, with the areas near the Tropics associated with higher processing water volumes. We suggest using this model combined with field-specific meteorological data to calculate a more accurate evaporation rate within acceptable errors. Also, it is important to point out that the numerical simulations discussed in this work are based on the parameters identified for a "reference evaporation surface". In order to obtain a suitable water supply in 2D SIE technology, porous media is generally selected as the material for the evaporator. The parameters utilized for the "reference evaporation surface" assumed that the evaporator consists of such porous medium. Nevertheless, the model can be easily extended and adjusted, as it allows changing these parameters to make predictions suitable for specific materials. Furthermore, estimations based on different surfaces may be compared to those obtained with such "reference evaporation surface" to understand their potential and behavior with respect to a common standard.

4 Outlook

In order to achieve the global carbon neutrality in the second half of this century, it is necessary to adjust the energy mix and to enhance the utilization of renewable energy sources. 2D SIE technology is a highly promising renewable energy-powered technology: means to estimate pre-experimental evaporation rates for large-scale applications are important to determine the preliminary feasibility of this technique. Detailed efficiency estimates would involve site selection, site size, infrastructure input and costing, and many other aspects that are critical to the longevity of on-site facilities and worthy of further study by researchers. There are many factors in the evaporation process that are not fully understood for real environment, such as turbulence. Laboratory research should be strengthened with increasingly comprehensive and robust models, but in particular with real-world analysis, ideally using data provided by actual installations on a large scale and over a long period of time, a complex task that may require multidisciplinary cooperation.

ACKNOWLEDGMENT

This work was supported by the National Natural Science Foundation of China (52070134, 51678377), and Litree Purifying Technology Co., Ltd. (2021H012). The data used in this study were acquired as part of the mission of NASA's Earth Science Division and archived and distributed by the Goddard Earth Sciences (GES) Data and Information Services Center (DISC).

References

[1] L. Zhou, X. Li, G.W. Ni, S. Zhu, J. Zhu, The revival of thermal utilization from the Sun: interfacial solar vapor generation, National Science Review, 6 (2019) 562-578.

[2] P. Tao, G. Ni, C. Song, W. Shang, J. Wu, J. Zhu, G. Chen, T. Deng, Solar-driven interfacial evaporation, Nature Energy, 3 (2018) 1031-1041.

[3] C. Zhang, Y. Shi, L. Shi, H. Li, R. Li, S. Hong, S. Zhuo, T. Zhang, P. Wang, Designing a next generation solar crystallizer for real seawater brine treatment with zero liquid discharge, Nature Communications, 12 (2021) 998.

[4] C.J. Chen, Y.D. Kuang, L.B. Hu, Challenges and Opportunities for Solar Evaporation, Joule, 3 (2019) 683-718.

[5] H. Ghasemi, G. Ni, A.M. Marconnet, J. Loomis, S. Yerci, N. Miljkovic, G. Chen, Solar steam generation by heat localization, Nature Communications, 5 (2014) 4449.

[6] Z. Xie, Y. Duo, Z. Lin, T. Fan, C. Xing, L. Yu, R. Wang, M. Qiu, Y. Zhang, Y. Zhao, X. Yan, H. Zhang, The Rise of 2D Photothermal Materials beyond Graphene for Clean Water Production, Advanced Science, 7 (2020).

[7] X. Li, J. Li, J. Lu, N. Xu, C. Chen, X. Min, B. Zhu, H. Li, L. Zhou, S. Zhu, T. Zhang, J. Zhu, Enhancement of Interfacial Solar Vapor Generation by Environmental Energy, Joule, 2 (2018) 1331-1338.

[8] Z. Wang, T. Horseman, A.P. Straub, N.Y. Yip, D. Li, M. Elimelech, S. Lin, Pathways and challenges for efficient solar-thermal desalination, Science Advances, 5 (2019).

[9] W. Wang, Y. Shi, C. Zhang, S. Hong, L. Shi, J. Chang, R. Li, Y. Jin, C. Ong, S. Zhuo, P. Wang, Simultaneous production of fresh water and electricity via multistage solar photovoltaic membrane distillation, Nature Communications, 10 (2019).

[10] Y. Guo, X. Zhou, W. Shi, G. Yu, Materials for solar-powered water evaporation, Nature Reviews Materials, 5 (2020) 388-401.

[11] Y. Geng, W. Sun, P. Ying, Y. Zheng, J. Ding, K. Sun, L. Li, M. Li, Bioinspired Fractal Design of Waste Biomass-Derived Solar-Thermal Materials for Highly Efficient Solar Evaporation, Advanced Functional Materials, (2020).

[12] J. Tang, T. Zheng, Z. Song, Y. Shao, N. Li, K. Jia, Y. Tian, Q. Song, H. Liu, G. Xue, Realization of Low Latent Heat of a Solar Evaporator via Regulating the Water State in Wood Channels, Acs Applied Materials & Interfaces, 12 (2020) 18504-18511.

[13] S.-L. Wu, L.-N. Quan, Y.-T. Huang, Y.-T. Li, H.-C. Yang, S.B. Darling, Suspended Membrane Evaporators Integrating Environmental and Solar Evaporation for Oily Wastewater Purification, ACS Applied Materials & Interfaces, (2021).

[14] D.P. Storer, J.L. Phelps, X. Wu, G. Owens, N.I. Khan, H. Xu, Graphene and Rice-Straw-Fiber-Based 3D Photothermal Aerogels for Highly Efficient Solar Evaporation, Acs Applied Materials & Interfaces, 12 (2020) 15279-15287.

[15] S.M. He, C.J. Chen, Y.D. Kuang, R.Y. Mi, Y. Liu, Y. Pei, W.Q. Kong, W.T. Gan, H. Xie, E. Hitz, C. Jia, X. Chen, A. Gong, J.M. Liao, J. Li, Z.J. Ren, B. Yang, S. Das, L.B. Hu, Nature-inspired salt resistant bimodal porous solar evaporator for efficient and stable water desalination, Energy & Environmental Science, 12 (2019) 1558-1567.

[16] C. Song, D. Qi, Y. Han, Y. Xu, H. Xu, S. You, W. Wang, C. Wang, Y. Wei, J. Ma, Volatile-Organic-Compound-Intercepting Solar Distillation Enabled by a Photothermal/Photocatalytic Nanofibrous Membrane with Dual-Scale Pores, Environmental Science & Technology, 54 (2020) 9025-9033.
[17] B. Peng, Y. Gao, Q. Lyu, Z. Xie, M. Li, L. Zhang, J. Zhu, Cationic Photothermal Hydrogels with Bacteria-Inhibiting Capability for Freshwater Production via Solar-Driven Steam Generation, ACS Applied Materials & Interfaces, (2021).
[18] S.K. Patel, C.L. Ritt, A. Deshmukh, Z. Wang, M. Qin, R. Epsztein, M. Elimelech, The relative insignificance of advanced materials in enhancing the energy efficiency of desalination technologies, Energy & Environmental Science, 13 (2020) 1694-1710.
[19] X. Li, G. Ni, T. Cooper, N. Xu, J. Li, L. Zhou, X. Hu, B. Zhu, P. Yao, J. Zhu, Measuring Conversion Efficiency of Solar Vapor Generation, Joule, 3 (2019) 1798-1803.
[20] Z. Chen, Y. Lin, Q. Qian, P. Su, Y. Ding, P.D. Tuan, L. Chen, D. Feng, Picosecond laser treated aluminium surface for photothermal seawater desalination, Desalination, 528 (2022) 115561.
[21] W. Yao, X. Li, X. Zhu, L. Pei, G. Liu, Y. Cheng, M.O.L. Chee, P. Dong, J. Shen, M. Ye, Thermal-localized and salt-resistant polyacrylonitrile/polyvinylidene fluoride aerogel for efficient solar desalination, Desalination, 532 (2022) 115751.
[22] N. Xu, J. Li, Y. Wang, C. Fang, X. Li, Y. Wang, L. Zhou, B. Zhu, Z. Wu, S. Zhu, J. Zhu, A water lily–inspired hierarchical design for stable and efficient solar evaporation of high-salinity brine, Science Advances, 5 (2019) eaaw7013.
[23] S. Zheng, M. Yang, X. Chen, C.E. White, L. Hu, Z.J. Ren, Upscaling 3D Engineered Trees for Off-Grid Desalination, Environmental Science & Technology, 56 (2022) 1289-1299.
[24] J. Xu, Z. Wang, C. Chang, B. Fu, P. Tao, C. Song, W. Shang, T. Deng, Solar-driven interfacial desalination for simultaneous freshwater and salt generation, Desalination, 484 (2020) 114423.
[25] Z. Chen, Q. Li, X. Chen, Porous Graphene/Polyimide Membrane with a Three-Dimensional Architecture for Rapid and Efficient Solar Desalination via Interfacial Evaporation, ACS Sustainable Chemistry & Engineering, 8 (2020) 13850-13858.
[26] S.-L. Wu, L.-N. Quan, Y.-T. Huang, Y.-T. Li, H.-C. Yang, S.B. Darling, Suspended Membrane Evaporators Integrating Environmental and Solar Evaporation for Oily Wastewater Purification, ACS Applied Materials & Interfaces, 13 (2021) 39513-39522.
[27] D.-D. Han, Z.-D. Chen, J.-C. Li, J.-W. Mao, Z.-Z. Jiao, W. Wang, W. Zhang, Y.-L. Zhang, H.-B. Sun, Airflow Enhanced Solar Evaporation Based on Janus Graphene Membranes with Stable Interfacial Floatability, Acs Applied Materials & Interfaces, 12 (2020) 25435-25443.
[28] L. Yang, N. Li, C. Guo, J. He, S. Wang, L. Qiao, F. Li, L. Yu, M. Wang, X. Xu, Marine biomass-derived composite aerogels for efficient and durable solar-driven interfacial evaporation and desalination, Chemical Engineering Journal, 417 (2021) 128051.

[29] W. Xie, P. Tang, Q. Wu, C. Chen, Z. Song, T. Li, Y. Bai, S. Lin, A. Tiraferri, B. Liu, Solar-driven desalination and resource recovery of shale gas wastewater by on-site interfacial evaporation, Chemical Engineering Journal, (2021) 132624.

[30] P. Zhang, Q. Liao, H. Yao, Y. Huang, H. Cheng, L. Qu, Direct solar steam generation system for clean water production, Energy Storage Materials, 18 (2019) 429-446.

[31] Z. Zhang, X. Li, J. Yin, Y. Xu, W. Fei, M. Xue, Q. Wang, J. Zhou, W. Guo, Emerging hydrovoltaic technology, Nature Nanotechnology, 13 (2018) 1109-1119.

[32] M. Elimelech, W.A. Phillip, The future of seawater desalination: Energy, technology, and the environment, Science, 333 (2011) 712-717.

[33] A. Pistocchi, T. Bleninger, C. Breyer, U. Caldera, C. Dorati, D. Ganora, M.M. Millán, C. Paton, D. Poullis, F.S. Herrero, M. Sapiano, R. Semiat, C. Sommariva, S. Yuece, G. Zaragoza, Can seawater desalination be a win-win fix to our water cycle?, Water Research, 182 (2020) 115906.

[34] Y. Zhang, T. Xiong, D.K. Nandakumar, S.C. Tan, Structure Architecting for Salt-Rejecting Solar Interfacial Desalination to Achieve High-Performance Evaporation With In Situ Energy Generation, ADVANCED SCIENCE, 7 (2020).

[35] L. Zhu, M. Gao, C.K.N. Peh, G.W. Ho, Recent progress in solar-driven interfacial water evaporation: Advanced designs and applications, Nano Energy, 57 (2019) 507-518.

[36] C. Zhang, H.Q. Liang, Z.K. Xu, Z.K. Wang, Harnessing Solar-Driven Photothermal Effect toward the Water-Energy Nexus, Advanced Science, 6 (2019).

[37] R.K. Vinukollu, E.F. Wood, C.R. Ferguson, J.B. Fisher, Global estimates of evapotranspiration for climate studies using multi-sensor remote sensing data: Evaluation of three process-based approaches, Remote Sensing of Environment, 115 (2011) 801-823.

[38] K. Wang, R.E. Dickinson, A review of global terrestrial evapotranspiration: Observation, modeling, climatology, and climatic variability, Reviews of Geophysics, 50 (2012).

[39] P.J. Sellers, R.E. Dickinson, D.A. Randall, A.K. Betts, F.G. Hall, J.A. Berry, G.J. Collatz, A.S. Denning, H.A. Mooney, C.A. Nobre, N. Sato, C.B. Field, A. Henderson-Sellers, Modeling the Exchanges of Energy, Water, and Carbon Between Continents and the Atmosphere, Science, 275 (1997) 502-509.

[40] T.R. McVicar, M.L. Roderick, R.J. Donohue, L.T. Li, T.G. Van Niel, A. Thomas, J. Grieser, D. Jhajharia, Y. Himri, N.M. Mahowald, A.V. Mescherskaya, A.C. Kruger, S. Rehman, Y. Dinpashoh, Global review and synthesis of trends in observed terrestrial near-surface wind speeds: Implications for evaporation, Journal of Hydrology, 416-417 (2012) 182-205.

[41] R.G. Allen, L.S. Pereira, D. Raes, M. Smith, Crop evapotranspiration-Guidelines for computing crop water requirements-FAO Irrigation and drainage paper 56, Fao, Rome, 300 (1998) D05109.

[42] H.L. Penman, Natural evaporation from open water, bare soil and grass, Proceedings of the Royal Society of London. Series A. Mathematical and Physical Sciences, 193 (1948) 120-145.

[43] J.L. Monteith, Evaporation and environment, Symposia of the Society for Experimental Biology, 19 (1965) 205-234.
[44] T. Akinaga, S.C. Generalis, C. Paton, O.N. Igobo, P.A. Davies, Brine utilisation for cooling and salt production in wind-driven seawater greenhouses: Design and modelling, Desalination, 426 (2018) 135-154.
[45] J. Herman, W. Usher, SALib: an open-source Python library for sensitivity analysis, Journal of Open Source Software, 2 (2017) 97.
[46] Amy McNally NASA/GSFC/HSL (2018), FLDAS Noah Land Surface Model L4 Global Monthly 0.1 x 0.1 degree (MERRA-2 and CHIRPS), Greenbelt, MD, USA, Goddard Earth Sciences Data and Information Services Center (GES DISC), Accessed: [2021.9.24], 10.5067/5NHC22T9375G.
[47] C. Zhong, A. Zolfaghari, D. Hou, G.G. Goss, B.D. Lanoil, J. Gehman, D.C.W. Tsang, Y. He, D.S. Alessi, Comparison of the Hydraulic Fracturing Water Cycle in China and North America: A Critical Review, Environmental Science & Technology, 55 (2021) 7167-7185.
[48] H.E. Beck, N.E. Zimmermann, T.R. McVicar, N. Vergopolan, A. Berg, E.F. Wood, Present and future Köppen-Geiger climate classification maps at 1-km resolution, Scientific Data, 5 (2018) 180214.